Magnetic properties of RBzPy[Ni(α-tpdt)$_2$] (R = H, Br, F): effects of *cis–trans* disorder†‡

D. Belo,[ab] M. J. Figueira,[a] J. P. M. Nunes,[a] I. C. Santos,[a] L. C. Pereira,[a] V. Gama,[a] M. Almeida*[a] and C. Rovira[b]

Received 7th March 2006, Accepted 10th May 2006
First published as an Advance Article on the web 23rd May 2006
DOI: 10.1039/b603443h

Three new salts RBzPy$^+$[Ni(α-tpdt)$_2$]$^-$ (α-tpdt = 2,3-thiophenedithiolate, BzPy = benzylpyridine, R = H, Br, F) were prepared and structurally and magnetically characterized. A common structural feature of these compounds is the arrangement of the anions with thiophenic sulfur atoms connecting to a coordinating sulfur atom of a neighbouring anion, placed almost perpendicular to each other. The cations are positioned with the pyridine rings inserted between thiophenic rings of anions, maximizing π–π interactions. Depending on the cation substitution structural differences and variable degrees of *cis–trans* disorder in the anions are observed, which affect the magnetic properties. HBzPy[Ni(α-tpdt)$_2$] displays dominant ferromagnetic interactions and cluster glass behaviour at low temperatures, BrBzPy[Ni(α-tpdt)$_2$] shows dominant antiferromagnetic interactions with a magnetic anomaly at ~6 K and FBzPy[Ni(α-tpdt)$_2$] magnetic behavior is dominated by weak ferromagnetic interactions but without magnetic ordering down to 1.5 K.

Introduction

Square planar bisdithiolene transition metal complexes have attracted considerable interest as building blocks for molecular materials as they are versatile units presenting a wide range of oxidation states, coordination geometries and magnetic moments[1] and so far they have been able to provide several interesting unusual properties such as metallic behaviour[2] or even superconductivity,[3] third order non-linear optical properties[4] and ferromagnetism.[5]

In these complexes more extended and sulfur rich ligands are expected to enhance solid state interactions, essential to allow either higher electrical conductivity or higher magnetic transition temperatures. Following this strategy we succeeded in the preparation of a novel series of transition metal complexes based on thiophenedithiolate ligands, which indeed have shown interesting electrical and magnetic properties.[6,7] Using these ligands we have recently reported the synthesis and characterization of several decamethyl metallocenium salts with [Ni(α-tpdt)$_2$]$^-$ (α-tpdt = 2,3-thiophenedithiolate), where this paramagnetic anionic complex proved to be a suitable building block for materials with interesting magnetic properties.[8,9] Fe(Cp*)$_2$[Ni(α-tpdt)$_2$] and Mn(Cp*)$_2$[Ni(α-tpdt)$_2$] fully illustrate the behaviour found in these compounds: the first one displays metamagnetic behaviour below 2.56 K with a critical field of 600 G,[8] while the manganese salt is a frustrated magnet.[9] The [Ni(α-tpdt)$_2$]$^-$ anion exhibits a spin polarization effect, which makes the study of its salts particularly attractive since it opens the possibility of obtaining bulk ferromagnetism in cases where the supramolecular arrangements in the crystal favour the existence of an effective overlap between the positive spin density regions of one anion with a negative spin density region in the neighbouring anion.

In order to further explore the use of this Ni complex as a precursor in this type of molecular magnetic materials, we decided to study several salts of this anion, namely with different substituted benzopyridine cations (RBzPy$^+$, with R = Br, F, H). Previous studies with other transition metal bisdithiolene complexes have shown that this type of cation favours the segregated stacking of the cations and anions putting into evidence different kinds of magnetic interactions and ordering, critically depending on the anion overlap mode in the crystal structure.[10] In this paper we report the properties of three salts of the [Ni(α-tpdt)$_2$]$^-$ anion with substituted benzylpyridinium cations (RBzPy$^+$, with R = Br, F, H).

Results and discussion

Crystals of BzPy[Ni(α-tpdt)$_2$] (**1**), BrBzPy[Ni(α-tpdt)$_2$] (**2**) and FBzPy[Ni(α-tpdt)$_2$] (**3**) of quality suitable for structure determination by X-ray diffraction, were obtained using standard procedures. In all compounds the unit cell contains one independent dithiolate complex and one independent RBzPy cation, both placed in general positions. At variance with the structure of previously reported [Ni(α-tpdt)$_2$]$^-$ salts, in which the complex always exhibited a *trans* configuration,[8,9]

[a]*Dept. Química, Instituto Tecnológico e Nuclear/CFMCUL, P-2686-953 Sacavém, Portugal. E-mail: malmeida@itn.pt; Fax: +351219941455; Tel: +351219946171*
[b]*Institut de Ciència de Materials de Barcelona, (CSIC), Campus Universitari de Bellaterra, E-08193 Cerdanyola, Spain. E-mail: cun@icmab.es; Fax: +344-93-5805729; Tel: +344-93-5801853*

† This article is part of a themed issue on Molecular Magnetic Materials.

‡ Electronic supplementary information (ESI) available: CIF files for compounds **1**, **2** and **3**; table of selected bond distances within transition metal complexes in **1**, **2** and **3**; figure of possible interanionic contacts for **1**. See DOI: 10.1039/b603443h

 This journal is © The Royal Society of Chemistry 2006

in all the compounds reported here there is clear evidence for variable amounts of *cis–trans* disorder (Fig. 1). In **1** and **3** only one of the ligands shows disorder indicative of two possible conformations, however in quite different amounts: 77% *cis* in **3** and 83% *trans* in **1**. In **2** both ligands present disorder in the position of the thiophenic sulfur atoms. However this disorder is different in the two ligands. The two possible positions of the sulfur atom in one ligand, S3 and S30, have 47 and 53% occupation factors, while in the other ligand S70 and S6 have 81% and 19% occupation factors respectively. This indicates that in addition to *cis–trans* disorder in the complex there is ~20% orientation disorder.

The Ni–S bond distances, with averages of 2.164(2), 2.167(4) and 2.164(6) Å for **1**, **2** and **3** respectively, are typical of the Ni(III) dithiolates[11,12] and comparable to those previously reported in this anion.[8,9] The atomic bond lengths within the ligands have normal values. In all three structures the $Ni(\alpha\text{-tpdt})_2$ anion is almost planar, with a small tetrahedral distortion of the coordination geometry (Fig. 1) due to a small rotation of one ligand relative to the other along the long axis of the complex.

The cations present usual bond lengths but with variable orientations between benzyl and pyridine rings. The dihedral angles between the C15–C14–N reference plane and the benzene ring are 64.8°, 80.1° and 73.8°, while with the pyridine ring they are 32.3°, 29.5° and 83.7° for the $[BzPy]^+$, $[BrBzPy]^+$ and $[FBzPy]^+$ cations, respectively (Fig. 2).

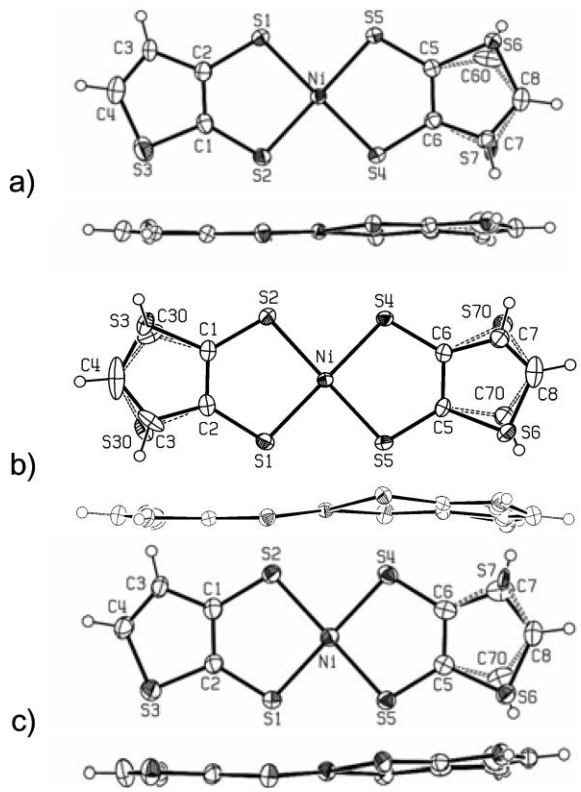

Fig. 1 ORTEP diagram at 40% probability and atomic numbering scheme of $[Ni(\alpha\text{-tpdt})_2]^-$ anion in the crystal structures of a) $BzPy[Ni(\alpha\text{-tpdt})_2]$ (**1**), b) $BrBzPy[Ni(\alpha\text{-tpdt})_2]$ (**2**) and c) $FBzPy[Ni(\alpha\text{-tpdt})_2]$ (**3**).

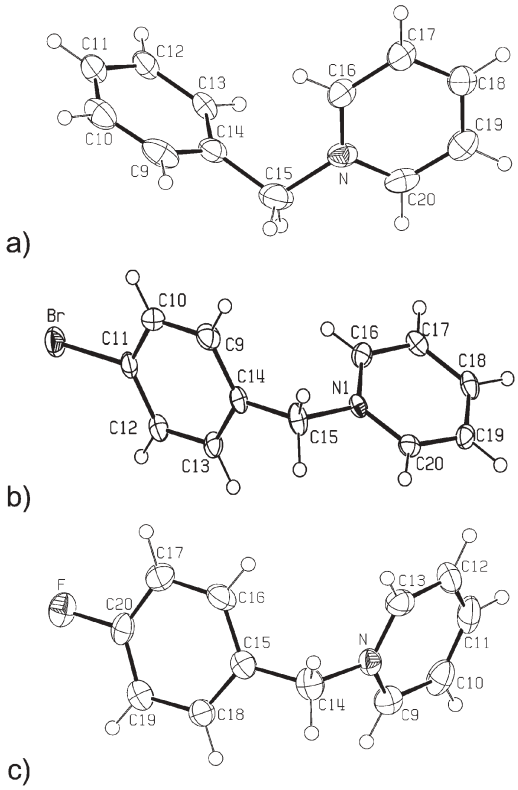

Fig. 2 ORTEP diagrams at 40% probability and atomic numbering schemes of $[RBzPy]^+$ cations in the crystal structures of a) $BzPy[Ni(\alpha\text{-tpdt})_2]$ (**1**), b) $BrBzPy[Ni(\alpha\text{-tpdt})_2]$ (**2**) and c) $FBzPy[Ni(\alpha\text{-tpdt})_2]$ (**3**).

The crystal structure of **1** is composed by double layers of anions parallel to the *a*,*b* plane separated by layers of cations (Fig. 3). The anion layers are composed by an almost square two dimensional array of the anions connected by short S1···S6 and S3···S4 contacts (Table 1), between coordination

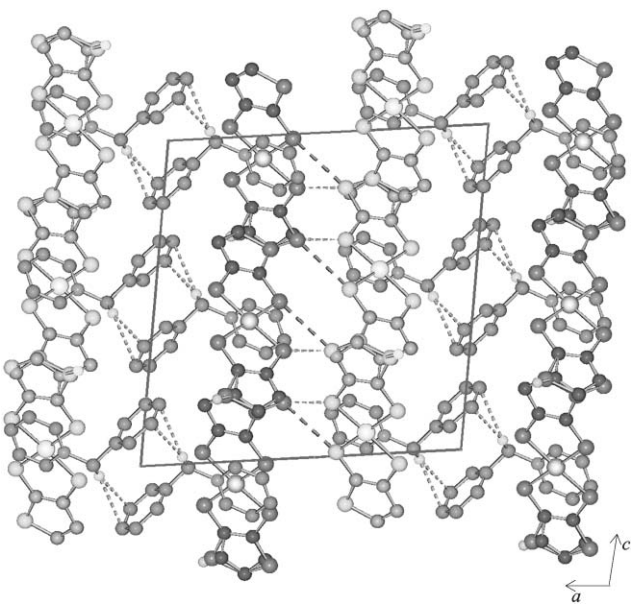

Fig. 3 Crystal structure of **1** viewed along *b*.

Table 1 Hydrogen bonds and short contacts in the crystal structure of **1**. If lower than 1 the occurrence probability is indicated in parentheses

	d/Å		Angle/°
S1···S6 (83%)[i]	3.497(2)	Within the layer	—
S3···S4[a] [ii]	3.741(1)	Within the layer	—
S2···S7 (17%)[iii]	3.555(20)	Between layers	—
S4···S7[a] (17%)[iii]	3.756(21)	Between layers	—
S5···H4–C4[iv]	2.89	Within the layer	161
S2···H8–C8[v]	2.98	Within the layer	158
S1···H9–C9[vi]	2.97	Anion–cation	152
S3···H18–C18[vii]	2.85	Anion–cation	148
S5···H13–C13[viii]	2.93	Anion–cation	167
S6···H11–C11[ix]	2.94	Anion–cation	131
C10···H15a–C15[x]	2.75	Cation–cation	162
C11···H15a–C15[x]	2.81	Cation–cation	142
C10···H12–C12i[x]	2.84	Cation–cation	157

[i] $x, -y - 0.5, z + 0.5$; [ii] $x, -y + 0.5, z + 0.5$; [iii] $-x + 1, y + 0.5, -z + 0.5$; [iv] $x, -y + 0.5, z - 0.5$; [v] $x, -y - 0.5, z + 0.5$; [vi] x, y, z; [vii] $-x + 1, -y + 1, -z + 1$; [viii] $x, y - 1, z$; [ix] $-x + 2, y - 0.5, -z + 0.5$, [x] $-x + 2, -y + 1, -z + 1$.

[a] 1% above the van der Waals radii sum.

and thiophenic sulfur atoms, the former occurring only 83% of the time, and also S···H–C hydrogen bonds (Fig. 4a). Due to the *cis–trans* disorder observed in the anion when S1···S6 is absent (17% of cases), two new S2···S7 and S4···S7 interaction between anion layers are established (Fig. 4b and Table 1). These are the only short contacts between the two anionic layers which are therefore relatively isolated, contacting for only 17% of the cases.

The cations have the pyridine rings inserted between thiophenic rings of the anions (Fig. 4a) and they are arranged in pairs due to a hydrogen bond assisting the overlap between the benzyl rings (Fig. 3 and Table 1).

The crystal structure of **2** is composed by alternating layers of anions and cations (Fig. 5), in a fashion similar to **1**. However a detailed analysis shows significant differences, certainly responsible for the different magnetic behaviour as described below. The double anionic layers in this compound have the anions much closer than in compound **1** and this double layer can be viewed as a layer of anionic pairs. The anions in these layers are organised in pairs, positioned side by side and connected by a short contact between coordination sulfur atoms S1···S5 (Table 2). This is in clear contrast with compound **1**, where the short interlayer contacts (S1···S6)

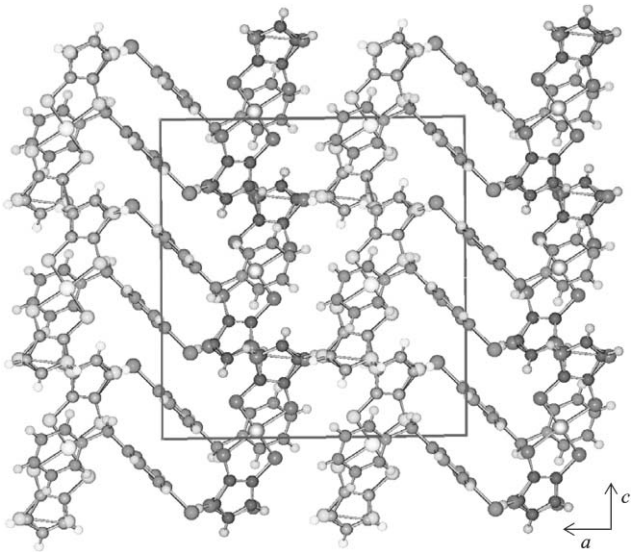

Fig. 5 Crystal structure of **2** viewed along *b*.

Table 2 Hydrogen bonds and short contacts in the crystal structure of **2**. If lower than 1 the occurrence probability is indicated in parentheses

	d/Å		Angle/°
S1···S5[i]	3.656(1)	Between layers[a]	—
S30···C5 (53%)[ii]	3.468(7)	Within the layer	—
S30···C6 (53%)[ii]	3.446(7)	Within the layer	—
S4···C4[ii]	3.832(4)	Within the layer	—
S70···C1 (81%)[iii]	3.528(8)	Within the layer	—
S4···Br[iv]	3.504(1)	Anion–cation	—
S70···Br (81%)[iv]	3.656(7)	Anion–cation	—
S70···C17 (81%)[v]	3.319(8)	Anion–cation	—
C5···C18[v]	3.294(4)	Anion–cation	—
C6···C17[v]	3.346(4)	Anion–cation	—
C7···C17[v]	3.371(7)	Anion–cation	—
S6···H17–C17[vi]	2.94	Anion–cation	143
S2···H9–C9[vii]	2.78	Anion–cation	173

[i] $-x + 1, -y + 1, -z + 1$; [ii] $x, -y + 0.5, z + 0.5$; [iii] $x, -y + 1.5, z - 0.5$; [iv] $-x, y + 0.5, -z + 0.5$; [v] $x, y + 1, z$; [vi] $-x + 1, y + 0.5, z + 0.5$; [vii] x, y, z.

[a] Within the pair.

involve pairs of anions that are nearly perpendicular as shown in Fig. 4. Neighbouring pairs are placed almost perpendicular to each other (the angle between the average planes of the

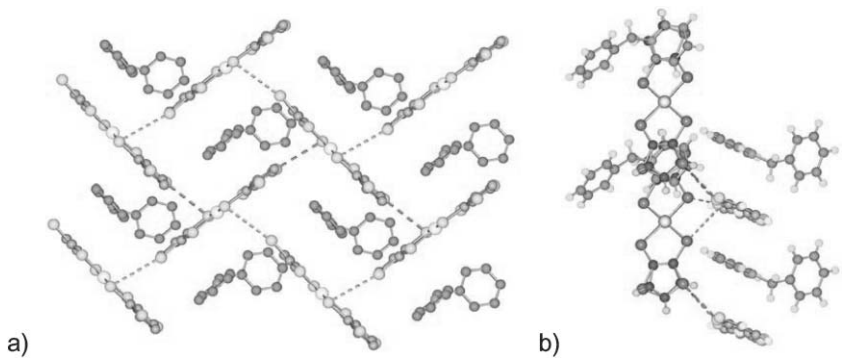

Fig. 4 Detail of the crystal structure of **1** a) view perpendicular to one anionic layer with cations inserted in the layer, b) detail showing the short contacts between anions in adjacent layers and the overlapping mode with anions.

 This journal is © The Royal Society of Chemistry 2006

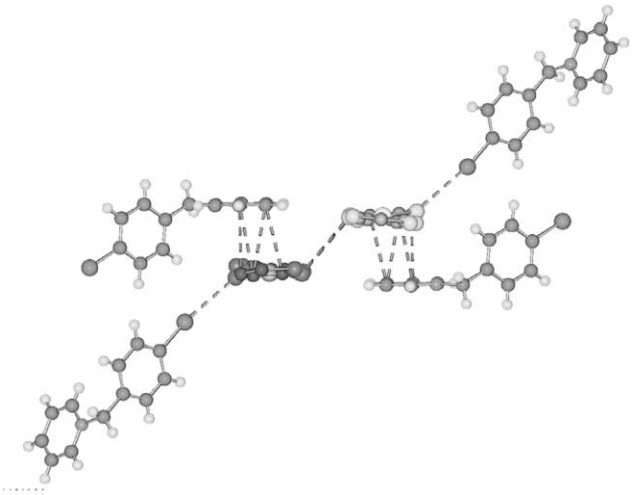

Fig. 6 Partial view of the crystal structure of **2**, showing the short S···S interaction within a pair of anions, the S···Br short contact and other interactions between anions and cations.

molecules is 76°) and the closest intermolecular distance is between the disordered thiophenic sulfur atom S70 and carbon atom C1. There are several interactions between anions and cations: two short S···Br contacts mediated by S4 and S70, a coordinating and a thiophenic sulfur atom respectively, C···C and C···S π–π interactions between the pyridine ring in the cation and the thiophenic ring in the anion, and several S···H–C hydrogen bonds (see Table 2). The cations act as linkers between anion layers since they interact through the bromide atom with one of the anions layer and, at the same time, interact through the pyridine ring with the thiophenic ring in the other anion layer (Fig. 6). While in **1** the shortest interaction contacts were associated with the "square" grid of each layer, in the structure of **2** there are shorter contacts associated with the pairs of anions in the double layers.

The crystal structure of **3** is again composed by alternated layers of anions and cations (Fig. 7), in a general fashion similar to **1** and **2**. However the anion layers consist of zig-zag chains of almost perpendicular $Ni(\alpha\text{-tpdt})_2$ anions (the angle between the molecules average plane is 86.6°) running along *b*. These chains are formed by anions connected by a short

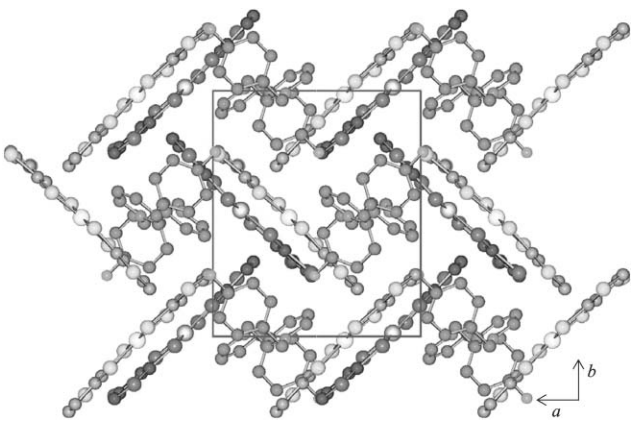

Fig. 7 Crystal structure of **3** viewed along *c*: chains in adjacent layers alternating in dark and light grey.

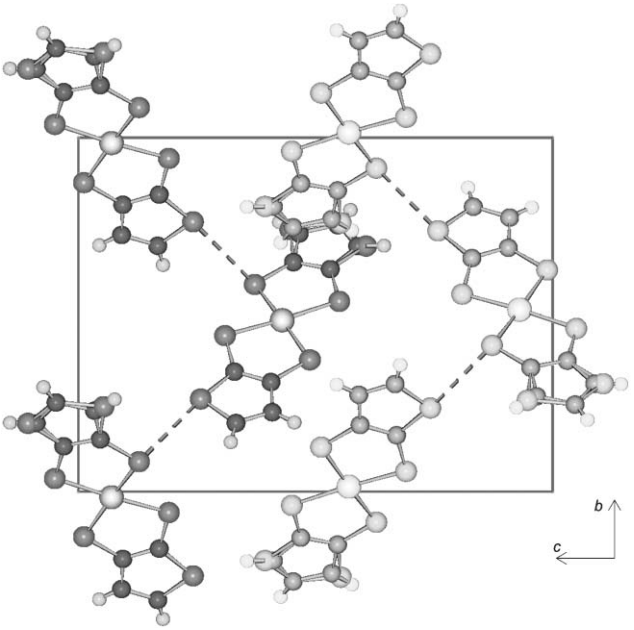

Fig. 8 View along *a* of the anions in **3** organized in two chains in adjacent layers (adjacent chains in dark and light grey).

S5···S3 interaction between a thiophenic and coordinating sulfur atom (Fig. 7 and 8). Neighbouring chains are connected also by short S···S contacts (Fig. 7 and Table 3).

The main interaction between chains, that occurs most often (77%), is also between thiophenic S6 and coordinating S4 sulfur atoms. However due to the *cis–trans* disorder this contact is broken in 23% of the cases and in those cases of *trans* configuration the chains are linked in the layers by both external thiophenic sulfur atoms throughout a S3···S7 short contact (Table 3). The anions in neighbouring chains are not positioned parallel to each other but slightly tilted (Fig. 8).

The anionic network gives rise to channels along *c*, which are occupied by the $FBzPy^+$ cations, strongly held by a charge assisted $C–F^{\delta+}\cdots S^{\delta-}$ interaction and several C–H···S hydrogen bonds (Fig. 7). This C–F···S interaction between anion and cation, which occurs for only 77% of the anions, is certainly responsible by the prevalence of the *cis* configuration.

Although at distances clearly above the sum of the van der Waals radii, the pyridine rings of the cations are sandwiched in

Table 3 Hydrogen bonds and short contacts in the crystal structure of **3**. If lower than 1 the occurrence probability is indicated in parentheses

	d/Å		Angle/°
S5···S3^{i}	3.508(2)	Within the chain	—
S4···S6 (77%)^{ii}	3.520(3)	Between chains	—
S3···S7 (23%)^{iii}	3.551(21)	Between chains	—
S6···F (77%)^{iv}	3.204(4)	Anion–cation	—
S3···H14a–C14^{v}	2.96	Anion–cation	116
S1···H17–C17^{vi}	2.94	Anion–cation	142
S6···H9–C9 (77%)^{vi}	2.98	Anion–cation	166
S7···H14b–C14 (23%)^{vii}	2.95	Anion–cation	122
F···H11–C11^{viii}	2.63	Cation–cation	138

^{i} $-x+1, y-0.5, -z+0.5$; ^{ii} $x-0.5, -y+0.5, -z$; ^{iii} $-x+1.5, -y+1, z+0.5$; ^{iv} $x+1, y, z$; ^{v} x, y, z; ^{vi} $-x+1, y+0.5, -z+0.5$; ^{vii} $-x+1.5, -y+1, z-0.5$; ^{viii} $x-0.5, -y+0.5, -z+1$.

between the thiophenic rings of the anions (Fig. 7) at 3.3 Å, but in this crystal structure the driving force in what concerns the interactions between anions and cations seems to be dominated by the S–F contact.

In these three compounds the crystal structure seems to be dominated by the packing pattern of anions, which tend to be positioned almost perpendicular to each other with a thiophenic sulfur connected to coordinating sulfur atoms. Additionally there is the above described *cis–trans* disorder to an extent which is expected to be sensitive to the crystallisation conditions.

As expected for Ni(III) in a square planar coordination geometry, these complexes are paramagnetic, with $S = 1/2$. For compound **1** the room temperature effective magnetic moment, μ_{eff}, of 1.6 μ_B is lower than the predicted value for independent $S = 1/2$ spins with $<g> = 2.07$, 1.79 μ_B. Fig. 9 shows the χT temperature dependence, where it is possible to observe first an increase of χT upon cooling.

The small μ_{eff} at room temperature and the increase of the χT product upon cooling suggest the coexistence of ferro- and antiferromagnetic interactions. At low temperatures, a field dependent maximum was observed in the magnetization. For a field of 20 G this maximum, T_f, occurs at 6.3 K and under increasing applied field it shifts to lower temperatures, and T_f = 6.1, 5.1 and 4.1 K, under 100, 350 and 850 G respectively. The ZFC and FC magnetization curves are coincident at high temperatures but become distinct below a temperature, T_i, just below T_f. Upon cooling, at lower temperatures, the FC curve passes through a minimum then it increases again while the ZFC curves decrease rapidly below the maxima, giving rise to a large difference between the ZFC and FC magnetisation. This suggests the occurrence of cluster glass behaviour in compound **1**.[13]

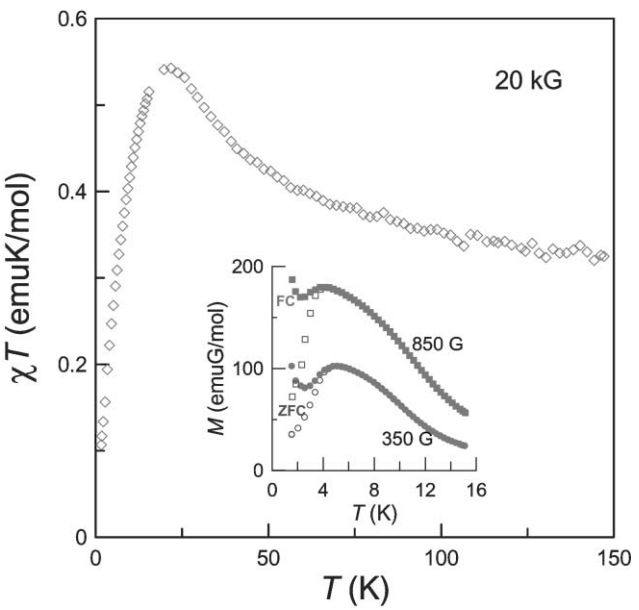

Fig. 9 Temperature dependence of χT for compound **1**, under an applied field of 20 kG. The inset shows the ZFC (open symbols) and FC (closed symbols) magnetization curves for applied fields of 350 and 850 G, represented by circles and squares respectively.

The magnetization curve obtained with a polycrystalline sample at 1.7 K is shown in Fig. 10. At this temperature even at fields as high as 120 kG the system is still far from saturation, M_s = 1.035 $N\mu_B$. The inset represents the magnetization curves as a function of H/T obtained at 1.7, 4.5, 8 and 15 K, as well as the calculated Brillouin function represented by a dashed line. It is possible to see that for the higher temperature (15 K) the experimental values are significantly larger than those calculated from the Brillouin function for a system of independent $S = 1/2$ spins. With cooling a significant decrease of the magnetization occurs, mainly for large H/T values, and for 1.7 K the magnetization exceeds the Brillouin function just for very low magnetic fields. A magnetisation cycle at 1.7 K is shown in Fig. 10b showing significant hysteresis. The hysteresis is of the order of 400 G between 500 and 2000 G, and it decreases drastically at low fields, becoming of the order of 40 G at zero field. At 1.7 K a small remnant magnetization, M_R, of the order of 0.003 $N\mu_B$ is detected.

At low temperatures AC susceptibility measurements revealed peaks both in the real and in the imaginary components. As shown in Fig. 11 there is a considerable frequency dependence of the maxima, $T_f(\omega)$.

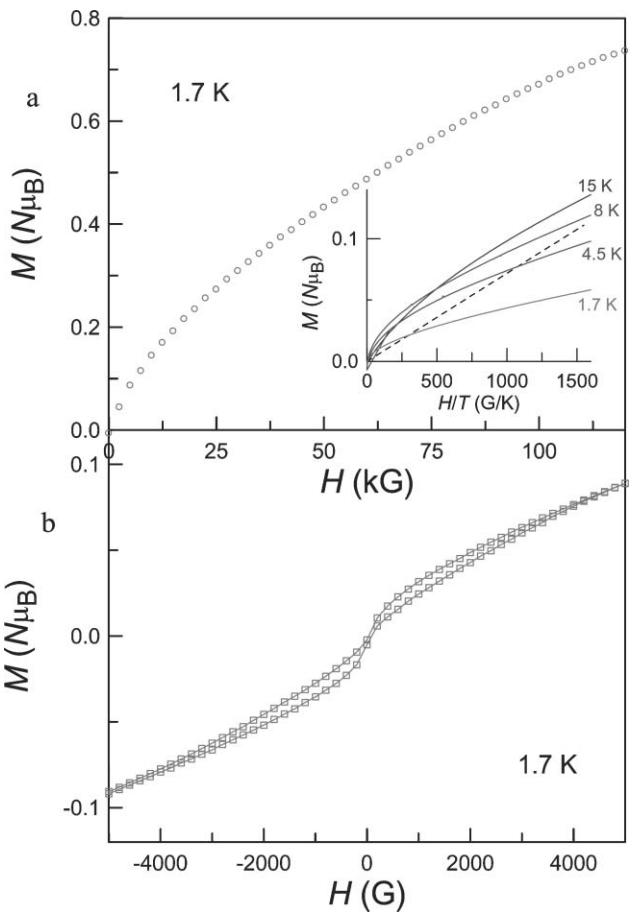

Fig. 10 (a) Magnetisation curve of **1**, at 1.7 K. The inset shows the magnetisation as a function of H/T at 1.7, 4.5, 8 and 15 K, as well as the calculated Brillouin function represented by the dashed line. (b) Magnetisation cycle at 1.7 K.

This journal is © The Royal Society of Chemistry 2006

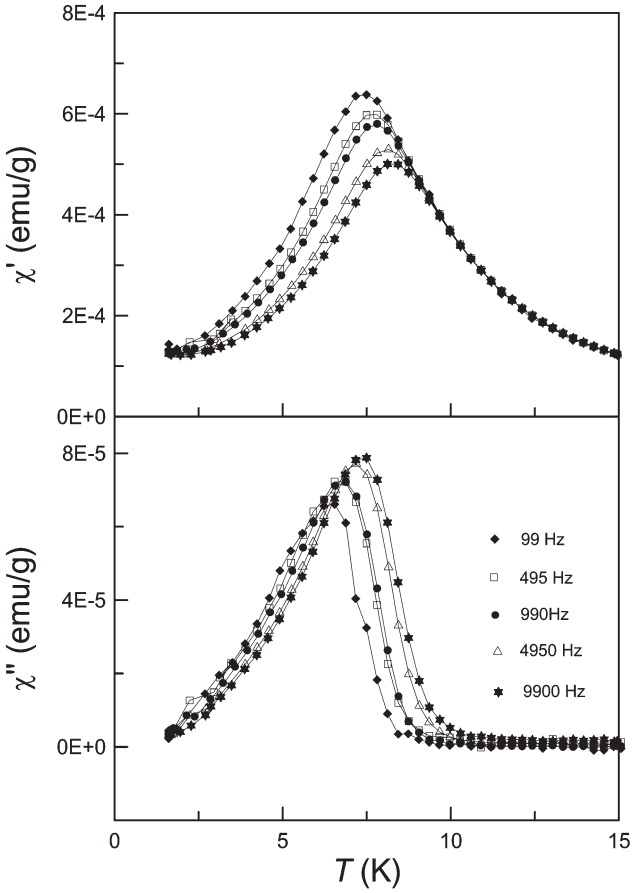

Fig. 11 (a) Real component of AC susceptibility, χ', temperature dependence for compound **1**. (b) Imaginary component, χ'', temperature dependence.

Both in the real and in the imaginary components the peaks shift to lower temperatures with decreasing frequencies. However the intensities of the peaks behave differently; While for the real component the intensity of the peaks increase with decreasing frequencies, in the imaginary component the peaks decreases with decreasing frequencies. This behaviour of χ' and χ'' is typical of a spin glass state. The frequency dependence of the peaks can be characterized through the parameter $\psi = (\Delta T_f/T_f)/\Delta(\log(\omega))$, which represents the relative shift of the freezing temperature per ω decade and for χ' $\psi = 0.05$, which is higher than the values observed in canonical spin glass systems, $\psi \sim 0.001$–0.01,[14] but lower than those observed in superparamagnets $\psi \sim 0.1$,[14] and the obtained ψ is consistent with cluster glass behaviour.

The frequency shift of the freezing temperature was analyzed through the Arrhenius law:

$$\omega = \omega_0 \exp[-E_a/k_B T_f] \quad (1)$$

where the frequency parameter is related to the magnetization relaxation time τ, by the relation $\tau = 1/\omega_0$, and E_a denotes an activation energy parameter. The values obtained from the Arrhenius law, $\omega_0 = 8.004 \times 10^{21}$ Hz ($\tau = 1.249 \times 10^{-22}$ s) and $E_a/k_B = 338.73$ K, are not physically appropriate. The results were also fitted with the Vogel–Fulcher law:

$$\omega = \omega_0 \exp[-E_a/k_B(T_f - T_0)] \quad (2)$$

where the parameter T_0, which accounts for the inter-cluster interaction, is introduced. In this case the obtained parameters $\omega_0 = 284.6$ MHz ($\tau = 3.513 \times 10^{-9}$ s), $E_a/k_B = 27.32$ K and $T_0 = 5.58$ K, seem to be physically appropriate. The obtained magnetization relaxation time, $\tau = 3.513 \times 10^{-9}$ s, lies in the range 10^{-6} to 10^{-13} s typical of cluster glass systems.[15] These results are consistent with the existence of significant inter-cluster interactions, as the parameter T_0 presents a value close to the freezing temperature, T_f.[16]

The McConnell I mechanism[17] has been by far the most popular model in the analysis of magnetic coupling in molecular materials. According to this model the nature of the magnetic intermolecular coupling is determined by the spin density (SD) signs in the atoms involved in the shorter intermolecular contacts. AFM coupling is predicted in cases where both atoms present the same sign of the SD and FM coupling is predicted in cases of different signs.

The $[Ni(\alpha\text{-tpdt})_2]^-$ anion is known to present a spin polarization effect, and the spin density distribution was calculated for the compound $[Fe(Cp^*)_2][Ni(\alpha\text{-tpdt})_2]$.[9] The calculated spin density distribution is shown in Fig. 12 for the *trans* configuration, and these calculations show these results are not significantly different for the *cis* configuration. In spite of its success the McConnell I mechanism has been questioned both theoretically[18] and experimentally.[19] Particularly in cases of competing intermolecular interactions (FM and AFM) the application of this mechanism can be easily misleading,[18] and the use of this model must consider its limitations. Nevertheless for a preliminary qualitative analysis it is not too bad and we will use it for a first structure–property correlation.

In the following discussion we will consider not only the closest intermolecular contact, but other close intermolecular contacts involving atoms with a significant spin density, and the magnetic coupling from each individual contact will be evaluated through two key factors: *i*, the spin density of the atoms involved in the contact; and *ii*, the interatomic overlap. In the following analysis the first (*i*) will be characterized by the product of the spin densities, sdP, of the atoms involved in the contact and the second (*ii*) will be primarily characterized by the parameter Q_W that represents the ratio between the interatomic separation, d, and the sum of the van der Waals radii of the atoms involved in the contact, d_W, $Q_W = d/d_W$.

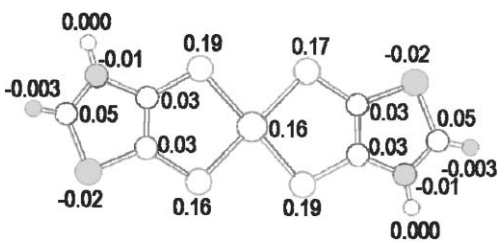

Fig. 12 Spin density distribution in the $[Ni(\alpha\text{-tpdt})_2]^-$ anion.

As previously mentioned the crystal structure of compound **1** consists of segregated layers of cations and anions and between the cation layers there is a pair of anionic layers. In this compound there is configurational disorder with the *trans* configuration being most probable (83%) and short contacts, between layers, are only observed when associated with the presence of the minority *cis* configuration (17%).

One anionic layer of compound **1** is shown in Fig. 4a. The thicker dashed lines correspond to the closer interanionic contacts S6···S1, with sdP $\cong -0.004$ and $Q_W = 0.95$. These contacts forming zig-zag chains are expected to give rise to FM coupling. Slightly longer contacts are observed between the chains, involving the similar atoms (S3···S4), with sdP $\cong -0.004$ and $Q_W = 1.01$. These intrachain contacts are represented by the thinner dashed lines in Fig. 4a. The anionic layers of compound **1** can be viewed as if the acceptors form zig-zag chains through interactions between the central MS_4 core of one anion and the extreme of the ligand in the neighbouring anion, and the anions placed nearly perpendicular to each other in layers of chains.

However due to the disorder in the structure, there is a significant number of breaks in those contacts due to the occurrence of the *cis* conformation with 17% probability. In cases of these breaks the coupling is expected to become AFM. In the case of the interchain and the interlayer contacts a competition between FM and AFM contacts is expected, however in both cases the nature of the dominant coupling is not clear. A detailed view of the intra and interchain as well as interlayer contacts is shown as electronic supplementary information (ESI).‡

The magnetic behaviour of this compound can be essentially related to the intrachain arrangement, where the chains in fact consist of a random sequence of AFM coupled zig-zag fragments, composed of a variable number of FM coupled $[Ni(\alpha\text{-tpdt})_2]^-$ units. Even disregarding any coupling between the chains, with cooling this system would freeze as a random distribution of clusters. The weaker interchain inter- and intralayer couplings are expected to be essentially determinant in the size of the clusters. Regarding the coupling between the clusters, it must be essentially determined by the chain breaks (AFM interactions), suggesting that the interactions between clusters must be AFM, which is in good agreement with the experimental results as during the freezing process a strong decrease of the magnetic moment is observed.

At room temperature the effective magnetic moment, μ_{eff}, of **2** is 1.4 μ_B, which is lower than that calculated, 1.79 μ_B, for a system of independent spins with $S = 1/2$ and $<g> = 2.07$. The low μ_{eff} value indicates the existence of strong antiferromagnetic exchange interactions between neighbouring $[Ni(\alpha\text{-tpdt})_2]^-$ anions. Fig. 13 shows the χT temperature dependence with an applied field of 30 kG. In spite of the dominant AFM interactions χT increases with cooling, showing a maximum at *ca.* 35 K, 0.320 emu K mol^{-1}, still considerably lower than that calculated for spin only ($S = 1/2$), 0.375 emu K mol^{-1}. The inset of Fig. 13 shows the paramagnetic susceptibility, for $T < 15$ K, under different applied magnetic fields. For low applied fields a local maximum is observed at *ca.* 5 K, and this maximum fades away with

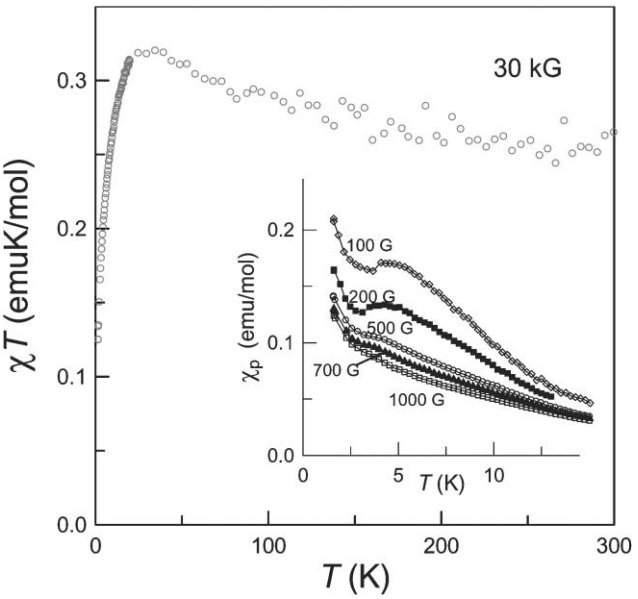

Fig. 13 Temperature dependence of χT for compound **2**. The inset shows the paramagnetic susceptibility behaviour for various applied fields.

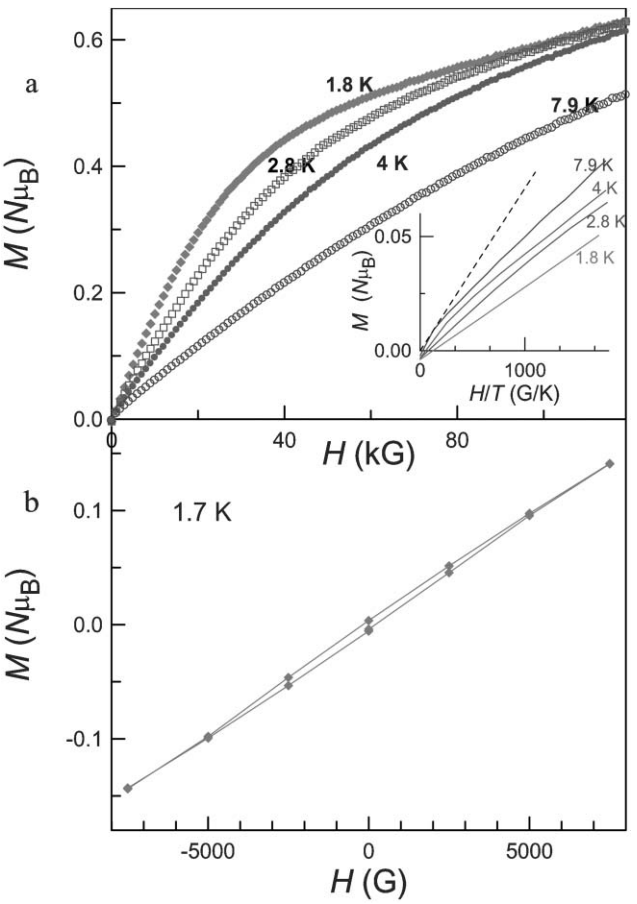

Fig. 14 (a) Magnetisation isotherms at various temperatures for compound **2**. The inset shows the magnetisation at different temperatures as a function of H/T, the dashed line being the Brillouin function. (b) Magnetisation cycle at 1.7 K.

This journal is © The Royal Society of Chemistry 2006

increasing applied fields turning into a shoulder in the susceptibility curves for fields higher than 500 G.

Fig. 14 shows the magnetisation curves of compound **2** obtained between 1.8 and 8 K. At lower temperatures ($T < 6$ K), the magnetization first increases rapidly with the magnetic field and at high fields shows a linear dependence with the applied field, which is reminiscent of canted AFM. However in such case the canting angle, θ, estimated according to the expression $M_s = M_s^c \sin\theta$,[20] where M_s^c is the calculated saturation magnetization, $M_s^c = gS = 1.035\ N\mu_B$ and M_s the saturation magnetisation, obtained from the value of the extrapolation from the linear regime to $H = 0$ ($M_s = 0.4\ N\mu_B$ at 1.8 K), leads to a totally unrealistic value of the order of 23°. Fig. 14b shows a magnetisation cycle, obtained at 1.7 K, with a hysteresis of the order of 500 G and a small remnant magnetization, M_R, of the order of 0.005 $N\mu_B$. As shown in the inset of Fig. 14a the magnetisation values at lower temperatures become gradually smaller than the Brillouin function, indicating dominant antiferromagnetic interactions. At 7.9 K for lower fields the magnetisation is still close to the calculated Brillouin function. However for lower temperatures the antiferromagnetic character becomes more pronounced.

AC susceptibility measurements at 1 kHz, with an AC field of 1 G and zero DC field, exhibit peaks both in the real, χ', and imaginary, χ'', components, as shown in Fig. 15. The maximum in χ' occurs at 7.9 K, while the maximum in χ'' is shifted to lower temperatures, at 6.6 K. The existence of peaks in both χ' and χ'' is consistent with the existence of weak ferromagnetism in this compound below $T_N = 7.9$ K, as suggested by the DC magnetisation measurements. Below the maximum in χ', at *ca.* 4 K, the susceptibility increases upon cooling, and the application of an external magnetic DC field decreases the intensity of the peak and shifts the maximum to lower temperatures. The peak in χ' seems to be suppressed for fields higher than 500 G, but it is just masked by the low temperature rise of χ', as the peak in χ'' is present with applied fields up to 1 kG, however this peaks loses intensity and shifts towards lower temperatures with higher DC magnetic fields.

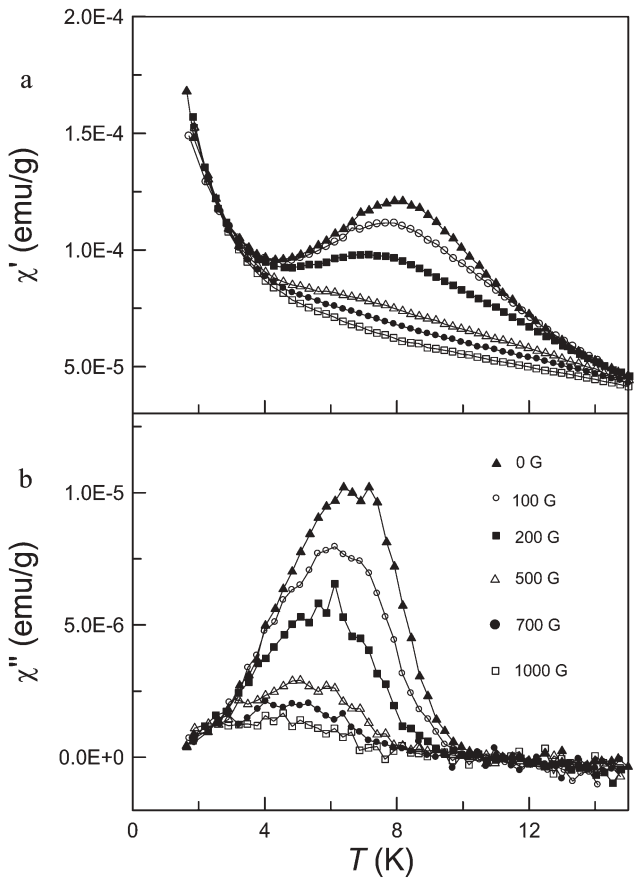

Fig. 15 Temperature dependence of real, χ', (a) and imaginary, χ'', (b) components of AC susceptibility of compound **2** under different indicated values of applied DC field.

In compound **2** a large structural disorder was observed; besides the *cis–trans* disorder, an orientation disorder is also present in this compound. This leads to the coexistence of four distinct conformations of the anions in the crystal structure of **2**. In the case of the *trans* configurations the most probable conformation T1 is associated with a probability of 46%, while the second conformation T2 has a probability of 8%. For the *cis* configuration the two possible conformations are C1 and C2 associated with probabilities of 35 and 11%.

The anionic arrangement within the layers, considering the most probable conformation (T1), is shown in Fig. 16; it exhibits the same general arrangement as that observed for compound **1**. The anions form zig-zag chains through C···S contacts, represented by the thick dashed lines in Fig. 16, involving one C from the thiophenic ring of one anion (C4) and one coordinating S from the adjacent anion (S4), for these contacts sdP $\sim$ 0.01 and $Q_W = 1.10$. There are similar contacts (C8···S1) between the chains, only slightly longer, $Q_W = 1.17$, represented by the thinner dashed lines. These contacts are shown in detail in Fig. 17a and are expected to lead to inter- and intrachain AFM coupling as the atoms involved in the contacts present positive spin densities.

As mentioned before, this compound exhibits a strong structural disorder and the analysis of all possible pair interactions requires the consideration of a large and

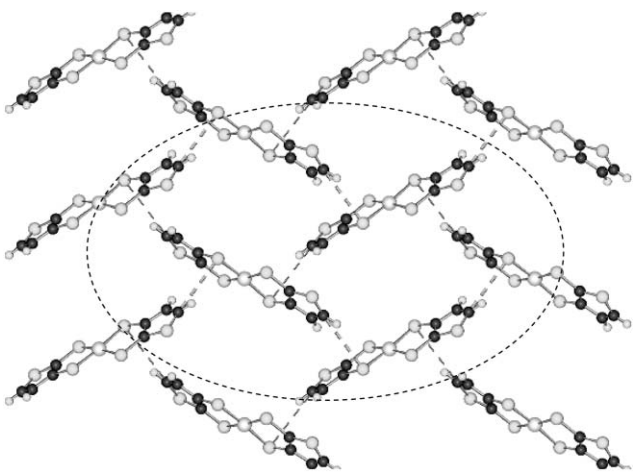

Fig. 16 The interanionic arrangements in one layer, associated with the most probable conformation (T1) for compound **2**. The thick dashed lines correspond to shorter intrachain contacts and the thin dashed lines to the shorter intrachain contacts.

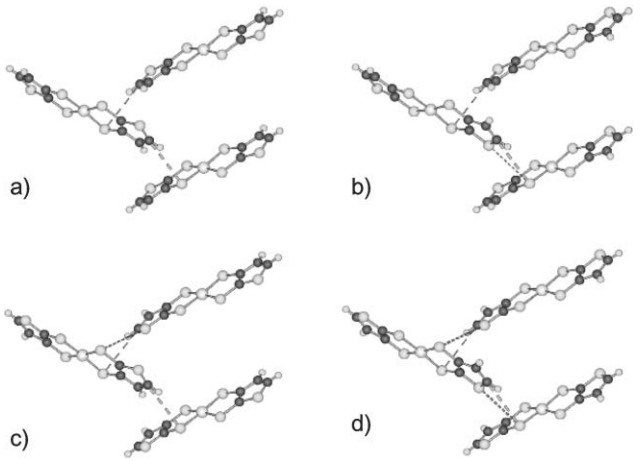

Fig. 17 The interanionic arrangements in one layer for compound **2**, associated with a) conformation T1 (46%), b) conformation C1 (35%), c) conformation C2 (11%) and d) conformation T2 (8%).

unpractical number of pairs. In this sense only arrangements with the simple *trans* (T1 and T2) and *cis* (C1 and C2) conformations will be analysed. It is worth mentioning that these "ordered" arrangements are a mere abstraction, since even for the most probable conformation, the existence of a T1T1 pair or a T1T1T1 trio have low probabilities, of the order of 21% and 10% respectively. A closer view of the various interanionic contacts is shown in Fig. 17 for the T1, T2, C1 and C2 conformations, concerning the intra- and the interchain contacts.

The contacts observed for the T1 conformation, shown in Fig. 17a, are present in the arrangements relative to all conformations, as it possible to observe in Fig. 17b, c and d, concerning conformations C1, C2 and T2 respectively. However, besides these contacts, new intra- and/or interchain contacts are observed in those conformations, which are represented by the short dashed lines. In the case of conformation C1, as shown in Fig. 17b, an extra intrachain contact is observed (S30···S4), with sdP ~ -0.0034 and Q_W = 1.07. In Fig. 17c the interanionic arrangement associated with the C2 conformation of the complexes is shown, and an extra interchain contact is observed (S70···S2), with sdP ~ -0.0034 and Q_W = 1.04. Finally in the arrangement corresponding to the T2 conformation of the complexes, shown in Fig. 17d, the extra intra- and interchain contacts previously mentioned (S30···S4 and S70···S2) are also present. The sdP of the new contacts is negative and they must give rise to FM interactions, competing with the permanent AFM contacts.

Within the layers, for compound **2**, in view of the limitations of the McConnell model, it is not possible to determine the dominant coupling between the anions, namely in the case of the interacting pairs where FM and AFM contacts coexist. However in view of the probabilities associated with the various conformations intrachain AFM coupling is expected for $\sim$57% of the pairs and interchain AFM coupling is expected for $\sim$81% of the anionic pairs. In this sense it is possible to expect that AFM coupling must be predominant both in the zig-zag chains and between the chains.

Unlike **1**, where the layers are relatively isolated, in compound **2** the anions in adjacent layers present nearly a side-by-side arrangement, as illustrated in Fig. 6, with short interanionic separations, with sdP $\sim$ 0.03 and Q_W = 0.99. Therefore according to the McConnell model the magnetic behaviour of **2** is expected to be largely dominated by strong AFM contacts in these pairs of anions. However this is not consistent with the magnetic behaviour of this compound, namely the slight increase of the χT product with cooling, which suggests that FM intralayer interactions may play a non-negligible role. This leads us to believe that the interactions in the pairs of anions in adjacent chains can be considerable weaker than expected, which could be due to a poor overlap between the S atoms in the pairs. In this case the intralayer coupling, with coexisting AFM and FM interactions, would be dominant. The AFM coupling between the pairs of anions can be related to the low temperature magnetic behaviour below the anomaly detected at *ca.* 6 K, where the magnetizaton field dependence clearly shows an approach to AFM behaviour with cooling, as shown in the inset of Fig. 14a. The study of the magnetic relaxation at low temperatures may help to clarify the magnetic behaviour of this compound.

The paramagnetic susceptibility of **3** follows Curie–Weiss behaviour, with a positive θ of 1.8 K. The effective magnetic moment, μ_{eff}, of 1.7 μ_B is very close to the value of 1.79 μ_B predicted for independent S = 1/2 spins with $<g>$ = 2.07. In compound **3**, the small positive θ value indicates that the magnetic behaviour is dominated by weak ferromagnetic interactions, which is confirmed by the magnetisation curve at 1.7 K, shown in Fig. 18, where the experimental values are larger than those calculated from the Brillouin function for independent S = 1/2 spins with $<g>$ = 2.07. At 4 T the magnetization saturates at a value slightly smaller than the calculated saturation magnetization, $M_s^c = gS = 1.035\ N\mu_B$. AC magnetic susceptibility measurements show no sign of magnetic ordering down to 1.5 K. This absence of magnetic order at low temperatures is consistent with the weak magnetic interactions observed at high temperatures.

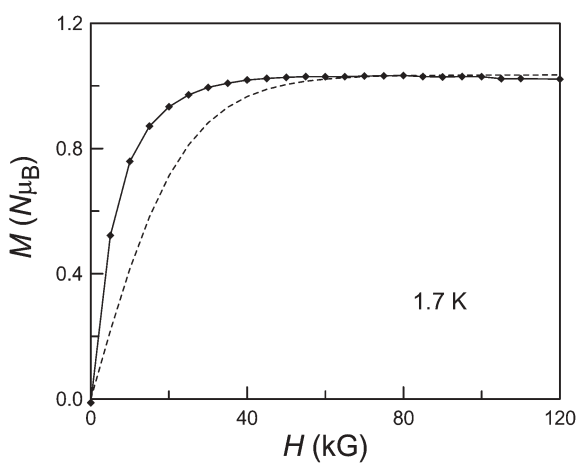

Fig. 18 Magnetisation isothermal of compound **3**, at 1.7 K. The dashed line represents the calculated values from the Brillouin function.

This journal is © The Royal Society of Chemistry 2006

In compound **3**, the shorter interanionic contact is between thiophenic S3 and coordinating S5 atom of the adjacent anion in the chain, with sdP $\cong -0.0034$ and $Q_W = 0.95$, and *cis–trans* disorder does not affect these contacts along the entire chain. These intrachain contacts are expected to lead to FM coupling since the atoms present different signs of the spin density.

The interchain contacts can be of two types depending on the *cis–trans* disorder. For the *cis* configuration, with a probability of 77%, there is the contact S6···S4 with sdP $\cong -0.0034$ and $Q_W = 0.95$ leading to FM coupling. For the *trans* configuration this contact is suppressed and instead contact S3···S7 is created, with sdP $\cong 0.0004$ and $Q_W = 0.95$, between side-by-side anions in adjacent chains. This contact, as it involves atoms with the same spin density parity, is expected to give rise to AFM coupling. One last short interchain contact C8···Ni was observed with sdP $\cong 0.008$ and $Q_W = 0.99$. This contact is present either in *cis* or *trans* conformations and it is expected to lead to AFM coupling since it involves atoms of the same SD parity.

In conclusion in this compound the intrachain interactions are expected to be FM while the interchain interactions have a competition between FM and AFM interactions. The small magnitude of these interactions and the significant disorder prevent ordering at lower temperatures.

Experimental

Synthesis

1-Benzylpyridinium salt of nickel(III) bis-2,3-thiophenedithiolate, BzPy[Ni(α-tpdt)$_2$] (1) (24 mg, 65%). To a solution of potassium methoxide in methanol (10 ml, 2 M) was added, under stirring, 5,6-thieno[2,3-*d*]-1,3-dithiol-2-one (25 mg, 1.4×10^{-5} mol). The formed yellow solution was filtered and added to a solution (2 ml) of nickel dichloride (27 mg, 7.1×10^{-5} mol) in methanol, where upon the colour changed to red. The inorganic precipitate was removed and the solution was taken out of the inert atmosphere and stirred in the open air in an ice bath, until the colour changed to green. This solution was, again, filtered and a solution of 1-benzylpyridinium bromide (23 mg, 7.1×10^{-5} mol) in methanol (5 ml) was added. A dark-green solid precipitated from the solution after cooling overnight. The solid was filtered and recrystallized from acetonitrile, and allowed to slowly evaporate, to afford dark-green plate crystals. The stirring was maintained, in all steps, until no visible modification was observed. CHNS Found C 46.29, H 2.92, N 2.43, S 36.66%; Calc for $C_{20}H_{16}NS_6Ni$: C 46.07, H 3.09, N 2.68, S 36.89%.

1-(4′-Bromobenzyl)pyridinium salt of nickel(III) bis-2,3-thiophenedithiolate, BrBzPy[Ni(α-tpdt)$_2$] (2) (32.8 mg, 77%). The synthetic method was the same as that used in the case of compound **1**, using 1-(4′-bromobenzyl)pyridinium bromide instead of 1-benzylpyridinium bromide. In this case a dark-green and shining solid precipitated from the solution, almost immediately after the addition of the cation. It was filtered and recrystallized from an acetone–ethanol 1 : 3 solution, and allowed to slowly evaporate, to afford dark-green plate crystals. CHNS Found C 39.33, H 3.20, N 2.18, S 32.83%; Calc for $C_{20}H_{15}NS_6NiBr$: C 40.02, H 2.52, N 2.33, S 32.04%.

1-(4′-Fluorobenzyl)pyridinium salt of nickel(III) bis-2,3-thiophenedithiolate, FBzPy[Ni(α-tpdt)$_2$] (3) (24.5 mg, 64%). The synthetic method was similar to that used in the case of compound **1**, using 1-(4′-fluorobenzyl)pyridinium bromide instead of 1-benzylpyridinium bromide. The best crystals, suitable for X-ray diffraction measurements, were obtained by recrystallisation from acetonitrile. CHNS Found C 44.06, H 3.51, N 2.10, S 36.01%; Calc for $C_{20}H_{15}NS_6NiF$: C 44.53, H 2.80, N 2.60, S 35.66%.

X-Ray structure determination

Diffraction data for compounds **1**, **2** and **3** were obtained with a Bruker AXS SMART APEX CCD detector diffractometer using graphite monochromatized MoKα radiation (λ = 0:71073 Å) at 130 K (**2**) and 110 K (for **1** and **3**) in the ϕ and ω scans. A semi-empirical absorption correction was applied with the program SADABS. The structures were solved by direct methods using SIR97[21] and refined by full-matrix least-squares methods using the program SHELXL97[22] and the winGX software package.[23] All non-hydrogen atoms were refined anisotropically. Hydrogen atoms were placed in idealised positions and allowed to refine riding on the parent C atom. The absolute structure determination of compound **2** was done in space group $P2_12_12_1$ which gave a Flack parameter of 0.5, indicative of racemic twinning. Molecular graphics were prepared using ORTEP 3[24] and SCHAKAL-99.[25] $NiS_6C_{20}H_{16}N$ (**1**), M = 521.41, monoclinic, $P2_1/c$, a = 14.9140(9) Å, b = 9.3980(7) Å, c = 15.3170(10) Å, β = 97.784(4)°, V = 2127.1(15) Å^3, μ = 1.508 cm^{-1}, Z = 4, D_{cal} = 1.628 g cm^{-3}, $R1$ = 0.0374, Rw = 0.0972, S = 1.056; $NiS_6C_{20}H_{15}BrN$ (**2**), M = 600.31, monoclinic, $P2_1/c$, a = 15.8727(2) Å, b = 8.30210(10) Å, c = 16.7073(2) Å, β = 90.2790(10)°, V = 2201.61(5) Å, μ = 3.274 cm^{-1}, Z = 4, D_{cal} = 1.811 g cm^{-3}, $R1$ = 0.0469, Rw = 0.1248, S = 1.044; $NiS_6C_{20}H_{15}FN$ (**3**), M = 539.40, orthorhombic, $P2_12_12_1$, a = 10.4280(12) Å, b = 12.3940(6) Å, c = 16.5940(19) Å, V = 2144.7(4) Å, μ = 1.506 cm^{-1}, Z = 4, D_{cal} = 1.671 g cm^{-3}, $R1$ = 0.0584, Rw = 0.1305, S = 0.988.

CCDC reference numbers 600731–600733. For crystallographic data in CIF or other electronic format see DOI: 10.1039/b603443h

Magnetic properties

The magnetic measurements, AC susceptibility and extraction magnetisation were performed on polycrystalline samples (10–15 mg) using a multipurpose characterization system, MagLab 2000 (Oxford Instruments) in the temperature range 1.7–300 K and with magnetic fields up to 120 kG. The magnetization data were corrected for contributions due to the sample holder and core diamagnetism estimated from tabulated Pascal constants as -2.5429×10^{-4}, 2.816×10^{-4} and 2.5766×10^{-4} emu mol^{-1} for **1**, **2** and **3** respectively.

Summary

In conclusion, three members of a new family of salts based on the $[Ni(\alpha\text{-tpdt})_2]^-$ anion and $RBzPy^+$ cations were prepared and characterised. In these compounds we observed, as a common structural feature, the tendency of the complexes to interact with neighbouring species *via* the thiophenic sulfur atom connecting to a coordinating sulfur atom in another complex, placing the complexes almost perpendicular to their next neighbours, in zig-zag chains. These chains are organized in an almost square lattice of anions approximately perpendicular to each other and perpendicular to the chain layers. This tendency contrasts with the stacking patterns so common in other bisdiothiolenes complexes and the benzylpyridine cations failed in promoting segregated anion stacking of $[Ni(\alpha\text{-tpdt})_2]^-$ anions.

In these complexes variable amounts of *cis–trans* disorder were found and most likely this percentage will depend on the crystallisation conditions. It is the first time that the *cis* configuration has been observed in this $[Ni(\alpha\text{-tpdt})_2]^-$ complex, and this appears as a consequence of preferential S···S interactions. The *cis–trans* disorder dominates the magnetic behaviour of these compounds.

$HBzPy[Ni(\alpha\text{-tpdt})_2]$ displays dominant ferromagnetic interactions and, as a consequence of more pronounced disorder effects, presents at lower temperatures behaviour typical of a cluster glass. $BrBzPy[Ni(\alpha\text{-tpdt})_2]$ shows dominant antiferromagnetic interactions with a magnetic anomaly at $\sim$6 K. The magnetic behaviour of $FBzPy[Ni(\alpha\text{-tpdt})_2]$ indicates weak ferromagnetic interactions but it remains a paramagnet down to 1.5 K.

This family of compounds shows how sensitive the magnetic properties can be to small changes within the building blocks and induced supramolecular interactions. The possibility of combining this anion with other substituted RR′BzPy cations in order to obtain new materials with different magnetic behaviours is currently being explored and will be reported in the future.

Acknowledgements

This work was partially supported by FCT under contract POCTI/QUI/45108/2002 and CICyT (MAT2003-04699). This work also benefited from COST action D35 and MAGMANet network of excellence.

References

1 (*a*) J. A. McCleverty, *Prog. Inorg. Chem.*, 1968, **10**, 29; (*b*) D. Coucuvanis, *Prog. Inorg. Chem.*, 1970, **11**, 233; (*c*) R. Eisenberg, *Prog. Inorg. Chem.*, 1970, **12**, 295; (*d*) L. Alcácer and H. Novais, in *Extended Linear Chain Compounds*, vol. 3, ed. J. S. Miller, Plenum Press, New York, 1983, ch. 6, p. 319; (*e*) S. Alvarez, V. Ramon and R. Hoffman, *J. Am. Chem. Soc.*, 1985, **107**, 6253.

2 (*a*) M. Ahamad and A. E. Hunderhill, *J. Chem. Soc., Chem. Commun.*, 1981, 67; (*b*) M. M. Ahamad, D. J. Turner, A. E. Hunderhill, C. S. Jacobsen, K. Mortensen and K. Carneiro, *Phys. Rev. B*, 1984, **29**, 4796.

3 P. Cassoux and L. Valade, in *Inorganic Materials*, 2nd edn, ed. D. W. Bruce and D. O'Hare, John Wiley and Sons, Chichester, 1996, pp. 1–64.

4 *Dithiolene Chemistry: Synthesis, Properties, and Applications*, ed. K. D. Karlin and E. I. Tiefel, *Progress in Inorganic Chemistry*, John Wiley & Sons, Chichester, 2004, vol. 52.

5 I. D. Parker, R. H. Friend, P. I. Clemenson and A. E. Hunderhill, *Nature (London)*, 1986, **324**, 547–548.

6 D. Belo, H. Alves, E. B. Lopes, M. T. Duarte, V. Gama, R. T. Henriques, M. Almeida, E. Ribera, C. Rovira and J. Veciana, *Chem.—Eur. J.*, 2001, **7**, 511–519.

7 D. Belo, M. J. Figueira, J. Mendonça, I. C. Santos, M. Almeida, R. T. Henriques, M. T. Duarte, C. Rovira and J. Veciana, *Eur. J. Inorg. Chem.*, 2005, 3337–3345.

8 D. Belo, H. Alves, S. Rabaça, L. C. Pereira, M. T. Duarte, V. Gama, R. T. Henriques, M. Almeida, E. Ribera, C. Rovira and J. Veciana, *Eur. J. Inorg. Chem.*, 2001, **9**, 3127.

9 D. Belo, L. Pereira, I. C. Santos, J. J. Novoa, V. Gama, M. Almeida and C. Rovira, submitted.

10 (*a*) J. L. Xie, X. M. Ren, C. He, Y. Song, C. Y. Duan, S. Gao and Q. J. Ming, *Polyhedron*, 2003, **22**, 299–305; (*b*) X. M. Ren, H. Okudera, R. K. Kremer, Y. Song, C. He, Q. J. Meng and P. H. Wu, *Inorg. Chem.*, 2004, **43**, 2569–2576; (*c*) Z. Ni, X. M. Ren, J. Ma, J. Xie, C. Ni, Z. Chen and Q. Meng, *J. Am. Chem. Soc.*, 2005, **127**, 14330.

11 W. E. Broderick, J. A. Thompson, M. R. Godfrey, M. Sabat and B. M. Hoffman, *J. Am. Chem. Soc.*, 1989, **111**, 7656.

12 C. Mahadevan, M. Seshasayer, P. Kuppusamy and P. T. Manoharan, *J. Crystallogr. Spectrosc. Res.*, 1985, **15**, 305–316.

13 (*a*) D. A. Pejakovic, J. L. Manson, J. S. Miller and A. J. Epstein, *Phys. Rev. Lett.*, 2000, **85**, 1994; (*b*) V. Turskan, M. Baran, R. Szymczak and R. Tidecks, *Physica B (Amsterdam)*, 2001, **296**, 301.

14 J. A. Mydosh, *Spin Glasses: An Experimental Introduction*, Taylor & Francis, London, 1993.

15 B. Antic, G. F. Goya, H. R. Rechenberg, V. Kusigerski, N. Jovic and M. Mitric, *J. Phys.: Condens. Matter*, 2004, **16**, 651.

16 R. N. Bhowmik and R. Ranganathan, *J. Magn. Magn. Mater.*, 2002, **248**, 101.

17 H. M. McConnell, *J. Chem. Phys.*, 1963, **39**, 1916.

18 M. Deumal, J. J. Novoa, M. J. Beapark, P. Celani, M. Olivucci and M. A. Robb, *J. Phys. Chem. A*, 1998, **102**, 8404.

19 M. Deumal, J. Cirujeda, J. Veciana and J. J. Novoa, *Chem.—Eur. J.*, 1999, **5**, 1631.

20 (*a*) H. C. Ku, H. M. Luo, B. N. Lin, Y. P. Chi, Y. Y. Hsu, Y. P. Sun and T. J. Lee, *Physica B (Amsterdam)*, 2000, **284–288**, 1373–1374; (*b*) H. M. Luo, Y. Y. Hsu, B. N. Lin, Y. P. Chi, T. J. Lee and H. C. Ku, *Phys. Rev. B: Condens. Matter Mater. Phys.*, 1999, **60**, 13119.

21 A. Altomare, M. C. Burla, M. Camalli, G. Cascarano, G. Giacovazzo, A. Guagliardi, A. G. G. Moliterni, G. Polidori and R. Spagna, *J. Appl. Crystallogr.*, 1999, **32**, 115.

22 G. M. Sheldrick, SHELXL97, A Program for Crystal Structure Refinement, University of Göttingen, Germany, 1997.

23 L. J. Ferrugia, *J. Appl. Crystallogr.*, 1999, **32**, 837.

24 L. J. Ferrugia, *J. Appl. Crystallogr.*, 1997, **30**, 565.

25 E. Keller, SCHAKAL-99, A Computer Program for the Representation of Molecular and Crystallographic Models, Kristallographisches Institut der Universität Freiburg, Germany, 1999.

This journal is © The Royal Society of Chemistry 2006